Original Paper

Landslides (2022) 19:2075–2090
DOI 10.1007/s10346-022-01901-y
Received: 7 April 2021
Accepted: 1 May 2022
Published online: 19 May 2022

Seungjun Lee · Hyunuk An · Minseok Kim · Giha Lee · Hongjoon Shin

Evaluation of different erosion–entrainment models in debris-flow simulation

Abstract Debris flow generated by landslides due to intense rainfall can cause extensive damage to residential areas. To predict and prevent the severity of such damage, several numerical models have been developed. However, there are limited studies regarding the entrainment and erosion effect of debris flow. This research aims to analyze several erosion–entrainment models for the selection of erosion–entrainment models in debris-flow analysis. The study focuses on landslides that occurred in the Raemian and Sindonga apartment basins in Mt. Umyeon, Republic of Korea, on July 27, 2011. The impact area, entrainment volume, maximum velocity, inundated depth, and erosion shape resulting from the debris-flow modeling were compared with field data. The simulation results of each erosion–entrainment model were assessed through the receiver operating characteristic method.

Keywords Landslides · Debris flow · Erosion–entrainment · Mt. Umyeon

Introduction

Debris flow, which comprises sediment and water, is typically triggered in steep landscapes due to high rainfall intensity and duration (Iverson 1997; Lai et al. 2018). This flow is capable of rapidly transporting large volumes of sediment and large boulders over long distances, making them destructive and dangerous (Coe et al. 2014; Takahashi 2007). Despite the significant danger and importance of landscape change (Stock and Dietrich 2003), limited work has been conducted to directly measure natural debris flows because they occur infrequently and are difficult, and dangerous, to measure (Kean et al. 2011; Takahashi 2007).

Numerical models are useful for analyzing the flow of difficult-to-implement mixtures, such as debris flows. In particular, for analyzing debris flow of high fluidity, caused by rainfall, rheological and entrainment models must be considered for numerical analysis. The rheological model dominates the overall flow of soil and has a significant effect on the flow velocity and the extent of the impact on an area. Moreover, erosion is a phenomenon in which topsoil is eroded due to debris flow, and entrainment refers to a phenomenon in which debris flow collects the eroded soil and the weakened topsoil during the flow process. Remaître et al. (2005) analyzed erosion process increases the volume of the collapsed soil 10–50 times. Pudasaini and Krautblatter (2021) figured out erosion–entrainment process determines the mobility and energy of the debris flow, and they explained the erosion–entrainment process full-mechanically first ever. Furthermore, this phenomenon has a significant effect on the damage caused to properties. Therefore, it is essential to apply the rheological model and the erosion–entrainment model to precisely analyze the extent of the damage, due to the debris flow, and caused to the surrounding area.

To analyze debris-flow hazards mechanism, many different one-dimensional (1D) or two-dimensional (2D) models have been proposed, and 2D simulations have provided strong insights into the dynamic behavior of debris flows (Denlinger and Iverson 2001; Pitman et al. 2003; Pudasaini et al. 2005; Richenmann et al. 2006; An et al. 2019; Liu and He 2020). Naef et al. (2006) compared several rheological models—Full Bingham, Simplified Bingham, Voellmy, Turbulent-Coulomb, Turbulent-Yield, Turbulent-Coulomb-Yield, Quadratic, and Coulomb-viscous—in a one-dimensional debris-flow simulation. In addition, several comparative studies of rheological models, in two-dimensional debris-flow simulations, were conducted (Medina et al. 2008; Bertolo and Bottino 2008; Christen et al. 2010; Pirulli 2010; Dahl et al. 2013). Furthermore, the performance of different debris-flow models or software such as DEFM-2D, FLO-2D, RAMMS, DAN, BING, Massflow, MassMov2D, MatDEM, and PFC was compared and explored (Rickenmann et al. 2006; Cesca and D'Agostino 2008; Pirulli and Sorbino 2008; Bertolo and Bottino 2008; Dahl et al. 2013; Scaringi et al. 2018). However, the performance of modeling the erosion–entrainment process has not yet been addressed through comparative studies, despite its importance.

To date, different erosion models have been derived from different theories and require different physical and nonphysical parameters. Takahashi and Nakagawa (1991) proposed an erosion–deposition model based on the concentration of the soil–water mixture with a number of physical parameters. Their model was derived from laboratory experimental studies and has deeper physical implications than the other erosion models. However, it requires an additional computation of the soil–water concentration, unlike the other models. McDougall and Hungr (2005) proposed an erosion–entrainment model in which the erosional rate is proportional to the flow depth and velocity and inversely proportional to the channel length. Sovilla et al. (2006) proposed a simple erosion–entrainment model in which the erosional rate is only proportional to the flow velocity in a snow avalanche simulation. In the approach proposed by Medinal et al. (2008), the erosional depth was derived based on the soil mechanics of the equilibrium between frictional forces (bed shear stress). Frank et al. (2015) computed the maximum erosion depth using the critical bed shear stress with the assumption of a constant erosion rate. Hong et al. (2020) simulated the soil entrainment process by combining the wetting front and Morgenstern's (1978) infinite slope stability model. With a seminal paper, Pudasaini and Fischer (2020) developed a fully mechanical erosion and deposition model based on the two-phase mass flow system by Pudasaini (2012). Pudasaini and Krautblatter (2021) proposed the first-ever physically correct and mathematically

consistent mechanical erosion–entrainment model for the energy budget of erosive landslides that controls their enhanced or reduced mobility, solving the long-standing problem in mass flow mobility. Recently, two-phase and multi-phase physics-based debris-flow models (Pudasaini 2012; Pudasaini and Mergili 2019) have been successfully applied to accurately simulate several complex catastrophic natural mass flow events (Mergili et al. 2020a, b; Shugar et al. 2021). Although several researchers successfully applied two-phase and multi-phase physics-based debris-flow models, these are still challenging because of their numerical complexity and the requirement of many physical parameters. Therefore, we limit ourselves to one-phase models and empirical erosion rates and modeling frames. Several methodologies have been proposed to simulate the erosion and entrainment phenomena that occur in the flow process. However, comparative analysis of each method is insufficient.

Therefore, the purpose of this study is a performance comparison of erosion–entrainment models conducted through a 2D debris-flow simulation. To do this, five models of the erosion–entrainment process, introduced by McDougall and Hungr (2005), Sovilla et al. (2006), static and dynamic equilibrium of Medina et al. (2008), and Frank et al. (2015), combined with three rheological models (Voellmy, Bingham, and Coulomb-viscous) were tested in a 2D debris-flow simulation. The impact area, entrainment volume, inundated depth, maximum velocity, and eroded depth were analyzed, and the comprehensive performances were compared based on the receiver operating characteristic (ROC) method introduced by Cepeda et al. (2010).

Materials and methods

Governing equation and numerical modeling

In this study, Deb2D, developed by An et al. (2019), was used to test the performance of the erosion–entrainment model in debris-flow simulation. This model can calculate the flow process faster than other numerical models because it simulates debris flows through an adaptive-mesh-refinement technique. The governing equation of Deb2D is a hyperbolic conservation form of the mass, and the momentum balance equation is expressed as follows:

$$\frac{\partial \mathbf{q}}{\partial t} + \frac{\partial \mathbf{f}}{\partial x} + \frac{\partial \mathbf{g}}{\partial y} = \mathbf{s}, \tag{1}$$

where t denotes the time, x and y are the Cartesian coordinates, and q, f, g, and s are the vectors representing conserved variables, fluxes in the x- and y-directions, and source terms, respectively. The vectors can be written as:

$$\mathbf{q} = \begin{pmatrix} h \\ hu \\ hv \end{pmatrix}, \ \mathbf{f} = \begin{pmatrix} hu \\ hu^2 + gh^2/2 \\ huv \end{pmatrix}, \ \mathbf{g} = \begin{pmatrix} hv \\ huv \\ hv^2 + gh^2/2 \end{pmatrix}, \ \mathbf{s} = \begin{pmatrix} E \\ S_{gx} - S_{fx} \\ S_{gy} - S_{fy} \end{pmatrix}, \tag{2}$$

where h is the depth of the debris-flow mixture, u and v are the depth-averaged velocity components in the x- and y-directions, respectively; g is the acceleration of gravity; E is the entrainment ($E > 0$) or deposition rate ($E < 0$); S_{gx} and S_{gy} represent the gravitational acceleration in the x- and y-directions, respectively; and S_{fx} and S_{fy} represent the driving friction in the x- and y-directions, respectively.

The Pudasaini (2012) and Pudasaini and Mergili (2019) multi-phase, multi-mechanical mass flow models based on the fully physically explained pressure- and rate-dependent Coulomb-viscoplastic rheological model cover all these aspects, and there are several successful application cases such as Mergili et al. (2020a, b) and Shugar et al. (2021). However, this study focuses on one-phase modeling approach due to the simplicity and applicability and widely used three rheological models, namely the Voellmy, Bingham, and Coulomb-viscous models, which are considered here.

First of all, the Voellmy friction is expressed as follows (Voellmy 1995):

$$S_{fx} = \mu_v gh + \frac{g|u|^2}{\xi}, S_{fy} = \mu_v gh + \frac{g|v|^2}{\xi}, \tag{3}$$

where a, the Coulomb friction coefficient, dominates the deceleration behavior when the flow is slow, and ξ, the turbulent friction coefficient, prevails when the flow is fast (Bartelt et al. 2013; Frank et al. 2015).

Second, the Bingham friction is expressed as follows (Bingham 1922):

$$S_{fx} = \frac{3}{\rho}\left(\frac{1}{2}\tau_c + \frac{\mu_b|u|}{h}\right), \ S_{fy} = \frac{3}{\rho}\left(\frac{1}{2}\tau_c + \frac{\mu_b|v|}{h}\right), \tag{4}$$

where ρ is the mass density, τ_c is the yield stress, and μ_b is the Bingham viscosity.

Lastly, the Coulomb-viscous friction is expressed as follows (Johnson and Rodine 1984):

$$S_{fx} = gh\ \tan\ \phi + \frac{3}{\rho}\left(\frac{1}{2}\tau_c + \frac{\mu_c|u|}{h}\right), \ S_{fy} = gh\ \tan\ \phi + \frac{3}{\rho}\left(\frac{1}{2}\tau_c + \frac{\mu_c|v|}{h}\right), \tag{5}$$

where ϕ is the friction angle between the bed material and surface and μ_c is the Coulomb-viscous viscosity.

The governing equation is discretized using the finite-volume method. Numerical models with shallow-water governing equations often suffer from an imbalance between the gradient of the water depth and bed slope in an irregular topography. This imbalance may cause numerical oscillations and instability in the simulation near shocks or wet–dry transitions. This model implements the hydrostatic reconstruction technique, proposed by Audusse et al. (2004), which has successfully been applied to quadtree adaptive grid-based shallow-water models. The discretized governing equation is calculated based on the HLLC scheme. Please refer to An et al. (2012) and An et al. (2019) for a detailed definition and calculation method for discrete terms.

Erosion–entrainment models

The importance of the erosion–entrainment phenomena, occurring in the progress of debris flow, has been identified in many previous studies (Medina et al. 2008; Frank et al. 2015; An et al. 2019; Pudasaini and Fischer 2020; Pudasaini and Krautblatter 2021). However, several approaches have been used, such as McDougall

and Hungr (2005); Sovilla et al. (2006); Medina et al. (2008); and Frank et al. (2015), although there is no study on performance analysis between each approach yet.

The erosional rate E in McDougall and Hungr (2005) is expressed as follows:

$$E(x,y,t) = \frac{\ln(V_f/V_0)}{\bar{S}} h\sqrt{u^2+v^2}, \tag{6}$$

where V_f is the final volume of debris flow, V_0 is the initial volume of debris flow, and $\bar{S}$ is the length of the channel. This approach requires the initial volume and final volume of debris flow, and these parameters are values that could acquire through field surveys. The entrainment rate a in Sovilla et al. (2006) is given as:

$$E(x,y,t) = \begin{cases} \kappa\sqrt{u^2+v^2} & \text{if) } h(x,y,0) - \int_0^t E(x,y,\epsilon)d\epsilon > 0 \\ 0 & \text{else} \end{cases}, \tag{7}$$

where κ is a dimensionless entrainment coefficient and $h(x,y,0)$ is the initial height of the entrainment layer at position (x, y). Note that Eq. (7) was originally proposed to simulate snow avalanches, but it has been successfully applied to debris-flow simulations (Hussin et al. 2012; An et al. 2019; Lee et al. 2020; Abraham et al. 2021).

Medina et al. (2008) proposed two erosion–entrainment models—static and dynamic equilibrium models—based on the soil mechanics of the equilibrium between frictional force and resistance force. The static equilibrium models are derived with the assumption of static flow and are given as follows:

$$E(x,y,t) = \frac{dz}{dt}, \tag{8}$$

$$h(x,y,0) = \begin{cases} \frac{S_f - S_b}{\rho g(\cos\theta\tan\varphi - \sin\theta)} & \text{if) } S_f > S_b \\ 0 & \text{else} \end{cases}, \tag{9}$$

$$S_b = c + \rho g h(1-\lambda)\cos\theta\tan\varphi, \tag{10}$$

where dz/dt is the erosion rate, S_b is the basal resistance force, θ is the angle between the horizontal plane and the velocity direction, φ is the bulk friction angle of the bed material, c is the cohesion, and λ is the pore pressure parameter, proposed by Iverson and Denlinger (2001). The dynamic equilibrium models are derived with the moving flow condition and expressed as follows:

$$E(x,y,t) = \frac{(S_f - S_b)}{\rho\sqrt{u^2+v^2}} \tag{11}$$

Note that the erosional rate is a constant parameter in the static equilibrium approach, whereas it has changed to a dynamic equilibrium approach in the aforementioned case. The model proposed by Frank et al. (2015) is as follows:

$$E(x,y,t) = \frac{dz}{dt}, \tag{12}$$

$$h(x,y,0) = \begin{cases} \frac{dz}{d\tau}(\tau - \tau_{fc}) = \frac{dz}{d\tau}(\rho g h s - \tau_{fc}) & \text{if) } \tau > \tau_{fc} \\ 0 & \text{else} \end{cases}, \tag{13}$$

where $dz/d\tau$ is the average potential erosion depth, τ is the shear stress, τ_{fc} is the critical shear stress, in the Frank algorithm, and s is the channel slope. This model also assumes a constant erosional rate, which is the same as that in the static equilibrium approach in Medina et al. (2008).

The five erosion–entrainment models were referred to in this study: McDougall and Hungr (2005); Sovilla et al. (2006); static and dynamic equilibrium models in Medina et al. (2008); and Frank et al. (2015). Figure 1 shows the flowchart of the Deb2D model.

Assessment of simulation results using ROC analysis

Godt et al. (2008) attempted ROC analysis to evaluate the accuracy of the simulation results in a landslide risk area analysis. Cepeda et al. (2010) proposed a quantitative method, using ROC analysis, to calibrate the parameters used in the debris-flow model. In this study, to evaluate the accuracy of the erosion–entrainment models, all models used parameters calibrated in each catchment. The required the true-positive rate (TPR), the false-positive rate (FPR), and error rate in ROC are given as follows (refer to Fig. 2a):

$$\text{TPR} = \frac{\text{TP}}{\text{TP}+\text{FN}},\ \text{FPR} = \frac{\text{FP}}{\text{FP}+\text{TN}},\ \text{error rate} = \sqrt{(1-\text{TPR})^2 + \text{FPR}^2} \tag{14}$$

The analysis of qualitative data, such as the impact area, is shown in Fig. 2b (Godt et al. 2008), and the analysis of quantitative data such as the flow velocity, inundated depth, and the entrainment volume uses the method proposed by Cepeda et al. (2010) (refer to Fig. 2c). The ROC is a method of estimating simulation results that are most suitable for field survey data among the simulation results. ROC compares implementation results with each other, so a direct comparison with observations is insufficient. Therefore, in this study, we tried to add an accuracy item (Acc.) that can directly compare observations and simulation results. The method of calculating Acc. is shown in Eq. (15), and the calculation method is divided into 1) the case of the impact area (qualitative data) and 2) the other case (quantitative data). To measure the overall accuracy, an error rate with accuracy (A.E rate) is computed as in Eq. (16).

$$\text{Acc.} = \begin{cases} \left|1 - \frac{\frac{\text{TP}+\text{TN}}{\text{P}+\text{N}}}{\frac{|\text{observed value} - \text{simulated result}|}{\text{observed value}}}\right| & \text{if) impact area} \\ & \text{else} \end{cases}, \tag{15}$$

$$\text{A.Erate} = \sqrt{(1-\text{Acc.})^2 + \text{error rate}^2} \tag{16}$$

TPR, FPR, and Acc. are calculated for each criterion, and appropriate weightings are assigned based on an expert assessment of the relative importance of each criterion (Cepeda et al. 2010). The accuracy of each model is assessed through the A.E rate, the combined data of Acc. and error rate. If the simulation and the actual event match perfectly, the A.E rate is zero.

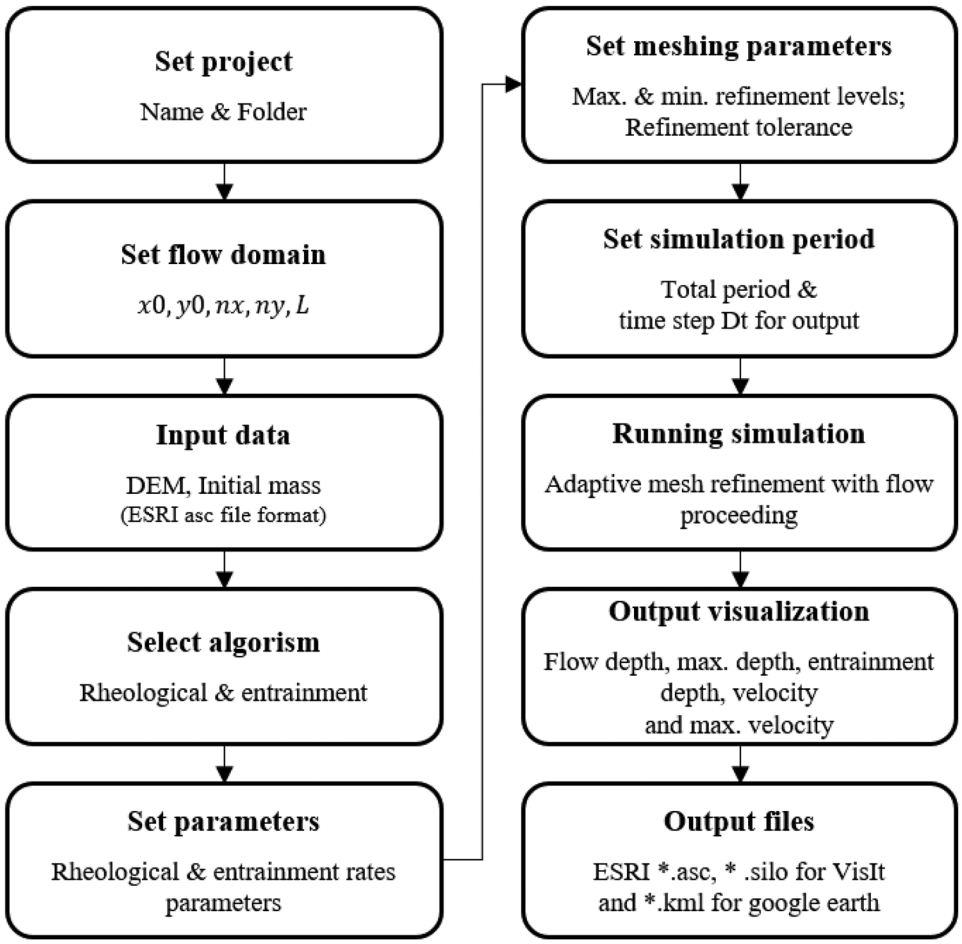

Fig. 1 Flowchart of the Deb2D model (modified from An et al. 2019)

Study area

In the Umyeon Mountain area, debris flows occurred due to torrential rainfall (rainfall amount: 500 mm/day; maximum rainfall intensity: 80 mm/h) on July 26 and 27, 2011. Mt. Umyeon is located in Seoul City. The water-laden debris flows inflicted significant property damage in the downtown areas, causing 16 deaths. Among a series of debris flows in the Mt. Umyeon area, field investigations and analysis using CCTV were conducted in the Raemian and Sindonga apartment basins. Field data are useful in the study of debris flow through back-analysis; therefore, we selected the Raemian and Sindonga basins to simulate the event.

According to a report (Seoul City 2014), debris flow occurred at four points (marked in red in the Raemian catchment) and three points in the Sindonga catchment through shallow landslides (Fig. 3). The observed channel lengths in the Raemian and Sindonga basins were reported to be 606 m and 664 m, respectively. The amount of eroded sediment (the final volume of debris flow) was 42,500 m^3 and 44,500 m^3, respectively. The maximum velocity of debris flows, which was analyzed using CCTV and dashboard

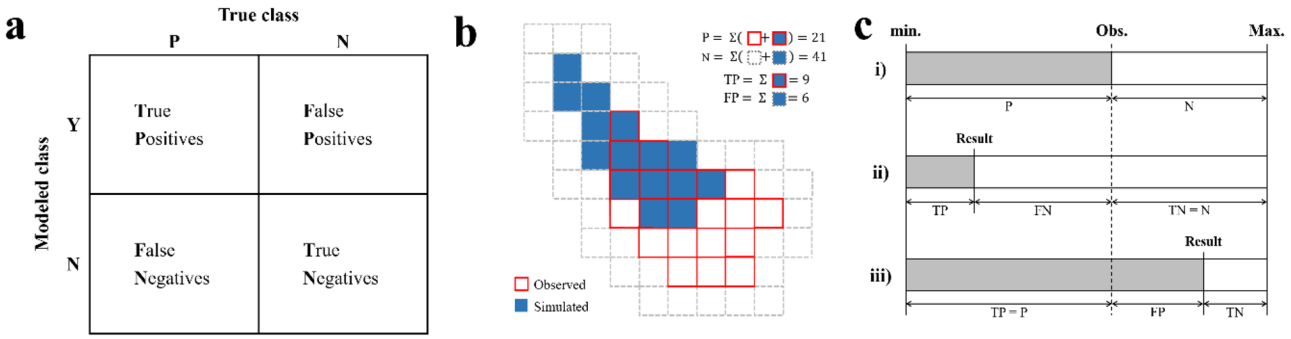

Fig. 2 (**a**) Confusion matrix showing outcome of a classification in ROC (modified from Fawcett 2006) and definition of variables for estimation of discrete classifiers for spatially distributed values (**b**) and for single-point scalar values (**c**) (modified from Cepeda et al. 2010)

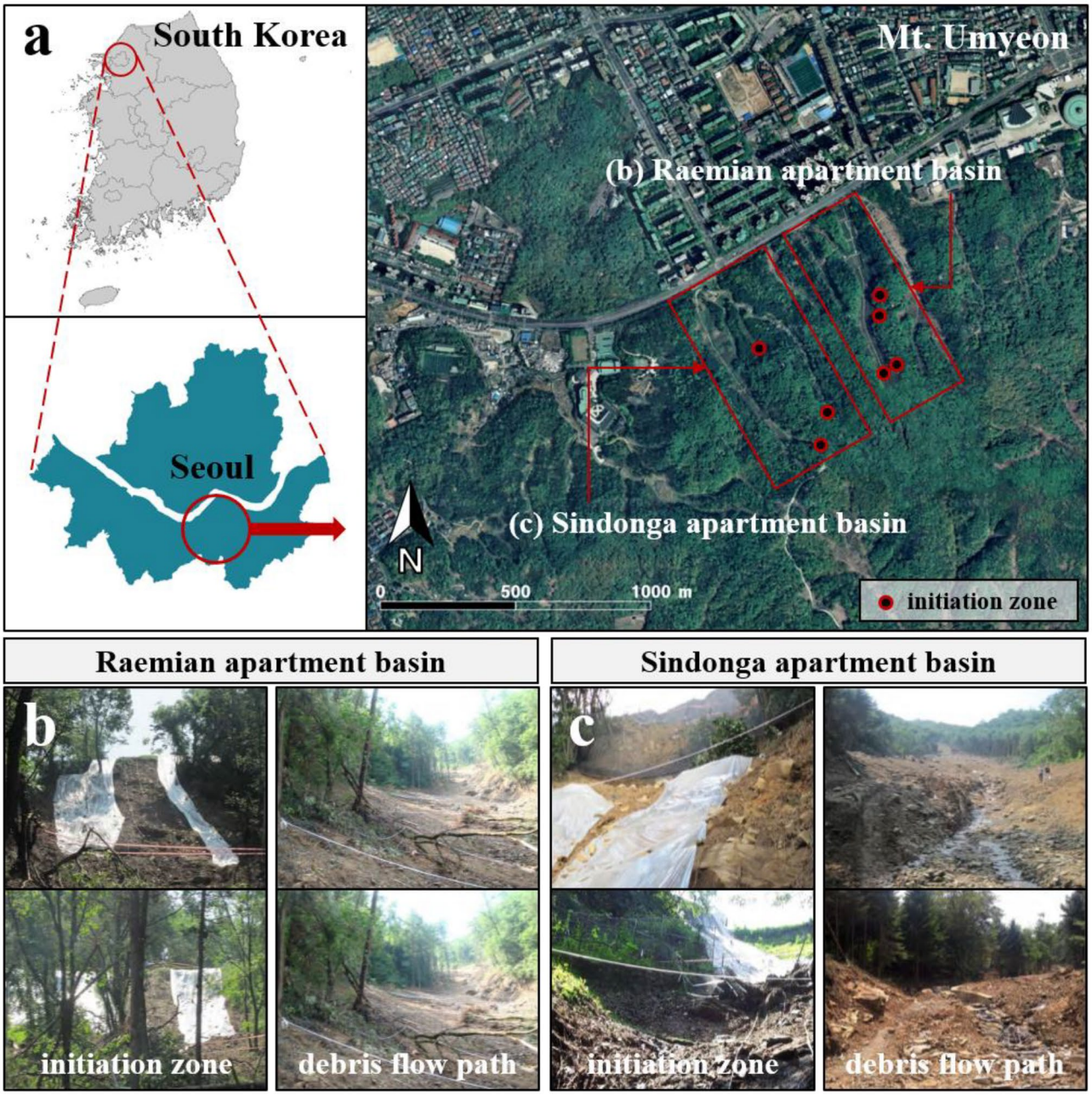

Fig. 3 (**a**) Study area and events: the 2011 landslide at Mt. Umyeon, Raemian apartment basin and Sindonga apartment basin, and digital photographs of Raemian apartment basin (**b**) and Sindonga apartment basin (**c**)

camera in a car, was estimated to be approximately 28 m/s and 18 m/s, at the Sindonga and Raemian apartment blocks, respectively. These debris-flow events were reported that caused direct damage to the third (approximately 10 m) and second (approximately 8 m) floors of Raemian apartment and Sindonga apartment, respectively, in the downtown area.

The mountain range is composed mainly of Precambrian banded biotite gneiss and granitic gneiss and has slopes with an average angle of 34°. In this study, the erodible soil depth is pre-determined by the report and field survey, which demonstrate that the erodible soil depth is distributed between 2 and 5 m (average 2 m). A digital elevation model, using light detection and ranging (LiDAR DEM) (1 m × 1 m), was used as the input data for the terrain. The scale of the collapse spots was constructed based on the difference in the LiDAR DEMs before and after the landslide. Therefore, the volumes on initial landslide scars were measured as 350 m^3 for both catchments.

Table 1 Estimation of discrete classifiers for the back analysis of the 2011 landslide at Raemian apartment catchment on the Mt. Umyeon using the sets of each erosion–entrainment model and the proposed ROC method

Raemian	Criterion →	Impact area (m^2)			Entrainment volume (m^3)			Inundated depth (m)			Max. velocity (m/s)			Total				
	w→	3			1			2			1							
		TPR	FPR	Acc.	TPR	FPR	Acc.	TPR	FPR	Acc.	TPR	FPR	Acc.	TPR	FPR	Acc.	error rate	A.E rate
Voellmy	McDougall and Hungr	0.598	0.053	0.925	0.890	0.000	0.990	1.000	0.000	1.000	0.000	0.000	0.536	0.669	0.023	0.900	0.332	0.346
	Sovilla	0.753	0.042	0.946	1.000	0.098	0.986	1.000	0.000	1.000	0.146	0.000	0.604	0.772	0.032	0.918	0.230	0.244
	Medina static	0.812	0.070	0.923	1.000	0.326	0.954	1.000	0.000	1.000	0.238	0.000	0.646	0.810	0.076	0.910	0.204	0.223
	Medina dynamic	0.843	0.029	0.963	1.000	0.195	0.972	1.000	0.000	1.000	0.308	0.000	0.679	0.834	0.040	0.934	0.171	0.183
	Frank	0.837	0.078	0.916	1.000	0.408	0.942	1.000	0.333	0.900	0.331	0.000	0.689	0.835	0.187	0.883	0.250	0.276
Bingham	McDougall and Hungr	0.863	0.055	0.940	1.000	0.025	0.997	1.000	1.000	0.700	0.354	0.000	0.700	0.849	0.313	0.845	0.347	0.380
	Sovilla	0.813	0.038	0.953	0.000	0.000	0.912	1.000	0.667	0.800	0.769	0.000	0.893	0.744	0.207	0.895	0.329	0.345
	Medina static	0.815	0.078	0.916	0.972	0.000	0.998	1.000	0.667	0.800	0.662	0.000	0.843	0.868	0.224	0.884	0.260	0.284
	Medina dynamic	0.808	0.044	0.946	0.852	0.000	0.987	0.000	0.000	0.910	0.785	0.000	0.900	0.580	0.019	0.935	0.420	0.425
	Frank	0.818	0.071	0.922	1.000	0.180	0.975	1.000	0.667	0.800	0.646	0.000	0.836	0.872	0.247	0.882	0.278	0.302
Coulomb	McDougall and Hungr	0.878	0.060	0.936	1.000	0.231	0.967	1.000	0.667	0.800	0.338	0.000	0.693	0.853	0.249	0.867	0.289	0.318
	Sovilla	0.816	0.038	0.953	0.613	0.000	0.966	1.000	0.667	0.800	0.762	0.000	0.889	0.832	0.207	0.902	0.266	0.284
	Medina static	0.814	0.074	0.919	0.486	0.000	0.955	1.000	0.667	0.800	0.769	0.000	0.893	0.814	0.222	0.886	0.290	0.311
	Medina dynamic	0.801	0.055	0.937	1.000	1.000	0.859	1.000	0.000	1.000	0.862	0.000	0.936	0.895	0.166	0.944	0.197	0.205
	Frank	0.818	0.075	0.918	0.842	0.000	0.986	1.000	0.667	0.800	0.731	0.000	0.875	0.861	0.223	0.888	0.263	0.285
Observation		45,820			42,500			10			28							

Table 2 Estimation of discrete classifiers for the back analysis of the 2011 landslide at Sindonga apartment catchment on the Mt. Umyeon using the sets of each erosion–entrainment model and the proposed ROC method

Sindonga	Criterion →	Impact area (m^2)			Entrainment volume (m^3)			Inundated depth (m)			Max. velocity (m/s)			Total				
	w →	3			1			2			1							
		TPR	FPR	Acc.	TPR	FPR	Acc.	TPR	FPR	Acc.	TPR	FPR	Acc.	TPR	FPR	Acc.	error rate	A.E rate
Voellmy	McDougall and Hungr	0.946	0.088	0.914	1.000	0.161	0.859	1.000	0.375	0.625	0.390	0.000	0.866	0.890	0.168	0.817	0.201	0.272
	Sovilla	0.815	0.123	0.874	1.000	0.919	0.418	0.000	0.000	0.863	0.000	0.000	0.780	0.492	0.184	0.792	0.540	0.579
	Medina static	0.835	0.140	0.859	1.000	0.374	0.735	0.182	0.000	0.888	0.439	0.000	0.876	0.615	0.113	0.852	0.401	0.427
	Medina dynamic	0.857	0.085	0.827	0.000	0.584	0.613	1.000	0.250	0.750	0.561	0.000	0.903	0.733	0.191	0.785	0.328	0.392
	Frank	0.837	0.157	0.843	1.000	0.148	0.867	0.909	0.000	0.988	0.244	0.000	0.833	0.796	0.088	0.886	0.222	0.250
Bingham	McDougall and Hungr	0.929	0.073	0.927	0.614	0.000	0.963	1.000	1.000	0.000	1.000	0.563	0.952	0.914	0.397	0.671	0.406	0.523
	Sovilla	0.747	0.075	0.919	0.000	0.000	0.829	0.818	0.000	0.975	0.268	0.000	0.839	0.592	0.032	0.911	0.409	0.419
	Medina static	0.862	0.139	0.861	0.692	0.000	0.980	1.000	0.063	0.938	0.415	0.000	0.871	0.813	0.077	0.901	0.202	0.225
	Medina dynamic	0.937	0.103	0.898	1.000	0.350	0.728	1.000	0.500	0.500	1.000	1.000	0.914	0.973	0.380	0.762	0.381	0.449
	Frank	0.866	0.155	0.845	1.000	0.053	0.922	1.000	0.025	0.975	0.488	0.000	0.887	0.869	0.081	0.899	0.154	0.184
Coulomb	McDougall and Hungr	0.960	0.082	0.919	0.957	0.000	0.962	1.000	0.750	0.250	0.732	0.000	0.941	0.938	0.249	0.737	0.257	0.368
	Sovilla	0.810	0.073	0.924	0.773	0.000	0.998	0.455	0.000	0.925	0.000	0.000	0.780	0.587	0.031	0.914	0.414	0.422
	Medina static	0.851	0.139	0.861	0.975	0.000	0.958	1.000	0.038	0.963	0.171	0.000	0.817	0.814	0.070	0.898	0.199	0.224
	Medina dynamic	0.844	0.095	0.903	1.000	0.054	0.921	1.000	0.375	0.625	1.000	0.875	0.925	0.933	0.281	0.829	0.288	0.335
	Frank	0.818	0.149	0.850	1.000	0.007	0.949	1.000	0.063	0.938	0.122	0.000	0.806	0.797	0.083	0.883	0.220	0.249
Observation		17,790			44,500			8			18							

Results

Three rheological models (Voellmy, Bingham, and Coulomb) and five erosion–entrainment models (McDougall and Hungr, Sovilla, Medina's static, Medina's dynamic, and Frank) were combined into 15 cases, as shown in Tables 1 and 2. According to Lee et al. (2020), the properties of the sediments, generated in the Raemian and Sindonga basins, were different. Therefore, in this study, parameter optimization was performed for each of the two basins for comparison and analysis.

Using the ROC method, the results were compared and analyzed using field data. The criteria were 1) the impact area, 2) the entrainment volume, 3) the inundated depth observed near the apartment, and 4) the maximum velocity of the debris flow observed near the road adjoining the apartments. The weight for each criterion was set by comprehensively assessing the reliability and importance of the field survey (Cepeda et al. 2010). Additionally, for the analysis of erosion, the erosion depth specific gravity graph, used by Frank et al. (2015), was also adopted in this work, and observational data were constructed using LiDAR DEMs before and after the landslide.

Raemian apartment basin

The results of the simulation of the Raemian catchment are summarized in Table 1, which shows the ROC for each erosion–entrainment model. The simulation using the Voellmy rheological model resulted in a value of 0.183–0.346 (average 0.254) for the A. E rate, which represents an overall higher achieved accuracy than the Bingham (0.284–0.425; aver. 0.347) and Coulomb (0.205–0.318; aver. 0.281) models. However, in all rheological models, it is difficult to implement the rapid flow velocity (28 m/s) of the Raemian basin debris flow. Here is because the observed flow velocity in this catchment is rapid compared with the previously studied debris-flow events. In particular, the Voellmy model exhibits lower accuracy than the other models at the flow velocity.

In the erosion–entrainment model, Medina's dynamic and static models had values of 0.183–0.425 (aver. 0.271) and –0.223–0.311 (aver. 0.273) for the A. E rate, respectively, demonstrating higher accuracy than other models such as McDougall and Hungr (0.318–0.380; aver. 0.348), Sovilla (0.244–0.345; aver. 0.291), and Frank (0.276–0.302; aver. 0.287). In particular, the Voellmy and Medina dynamic combination revealed the lowest the A. E rate (0.183), showing the highest accuracy; the next Coulomb and Medina dynamic combination was also found to be accurate, with an A. E rate of 0.205.

The simulated erosion data, according to the five erosion–entrainment models, are shown in Figs. 4 and 5. The McDougall and Hungr model indicates that erosion occurred in a larger area than observed, especially in the lower part of the basin (Fig. 4b). Sovilla and Medina's dynamic models (Fig. 4c and e) show that erosions occurred several times in the middle and upper parts of the basin. In addition, Medina's dynamic model revealed this phenomenon more extremely. Frank and Medina's static models revealed similar erosion patterns; however, the Frank model showed better performance in the middle and upper parts of the catchment (Fig. 4d and f). However, it was difficult to simulate erosion on the left side of the lower area of the basin in any entrainment model. This aspect seemed to be due to the limitation of DEMs precision by dense trees and narrow watershed.

In Fig. 5, the analysis graph, used by Frank et al. (2015), showed that the rheological model has an insignificant influence on the erosion process, and the selected erosion–entrainment model was important when simulating the erosion depth. The McDougall and Hungr and Sovilla models were found to have a deeper erosion depth than the observed data. Similar to the analysis in Fig. 4, Medina's static and Frank models generally exhibited patterns analogous to the observations. The result of the Voellmy and Frank combination, which is the maximum debris-flow depths in the Raemian basin, is shown in Fig. 6.

Sindonga apartment basin

The analysis of the Sindonga basin showing the ROC results for each erosion–entrainment model is shown in Table 2. The Coulomb rheological model revealed A. E rate of 0.224–0.422 (aver. 0.320), indicating greater accuracy than achieved by the Voellmy (0.250–0.579; aver. 0.384) and Bingham (0.184–0.523; aver. 0.360) models. The maximum velocity in the Sindonga basin was 18 m/s, which is lower than that in the Raemian basin. Therefore, it can be implemented well in each of the rheological models adopted within this study. However, criteria other than velocity showed lower accuracy than the Raemian catchment.

Medina's static and Frank models showed A. E rate of 0.224–0.427 (aver. 0.292) and 0.184–0.250 (aver. 0.228), respectively, showing higher accuracy than other models such as McDougall and Hungr (0.272–0.523; aver. 0.388), Sovilla (0.419–0.579; aver. 0.473), and Medina's dynamic (0.335–0.449; aver. 0.392). In particular, the Bingham and Frank combination showed the highest accuracy, with an A. E rate of 0.184, followed by the Coulomb and Medina's static combination with an A. E rate of 0.224.

The analysis of the erosion depth for the Sindonga catchment is shown in Figs. 7 and 8. McDougall and Hungr and Medina's dynamic models (Fig. 7b and e) showed that significant erosion occurred in the left catchment area. In Fig. 7c, d, and f, Sovilla, Medina's static, and Frank models exhibited erosion on the right side of the basin. McDougall showed similar erosion patterns to Sovilla and Medina's dynamic models, and unlike observations, it predicted that erosion would occur several times in the middle and upper parts. Overall, Medina's static and Frank models (Fig. 7d and f) showed high accuracy, and Medina's static and Frank models exhibited very comparable results. However, it is difficult to simulate erosion on the left side of the lower area of the catchment in any entrainment model.

In Fig. 8, McDougall and Hungr, Sovilla, and Medina's dynamic models showed an analogous pattern to that of the observation at a depth of more than 2 m; however, the analysis of the erosion depth of less than 2 m revealed low accuracy. Medina's static model showed different results, according to the rheological models, compared with other erosion–entrainment models. However, it was difficult to simulate a greater erosion depth even when combined with any rheological model. In the case of the Frank model, a low erosion depth of 1 m or less was implemented with high accuracy,

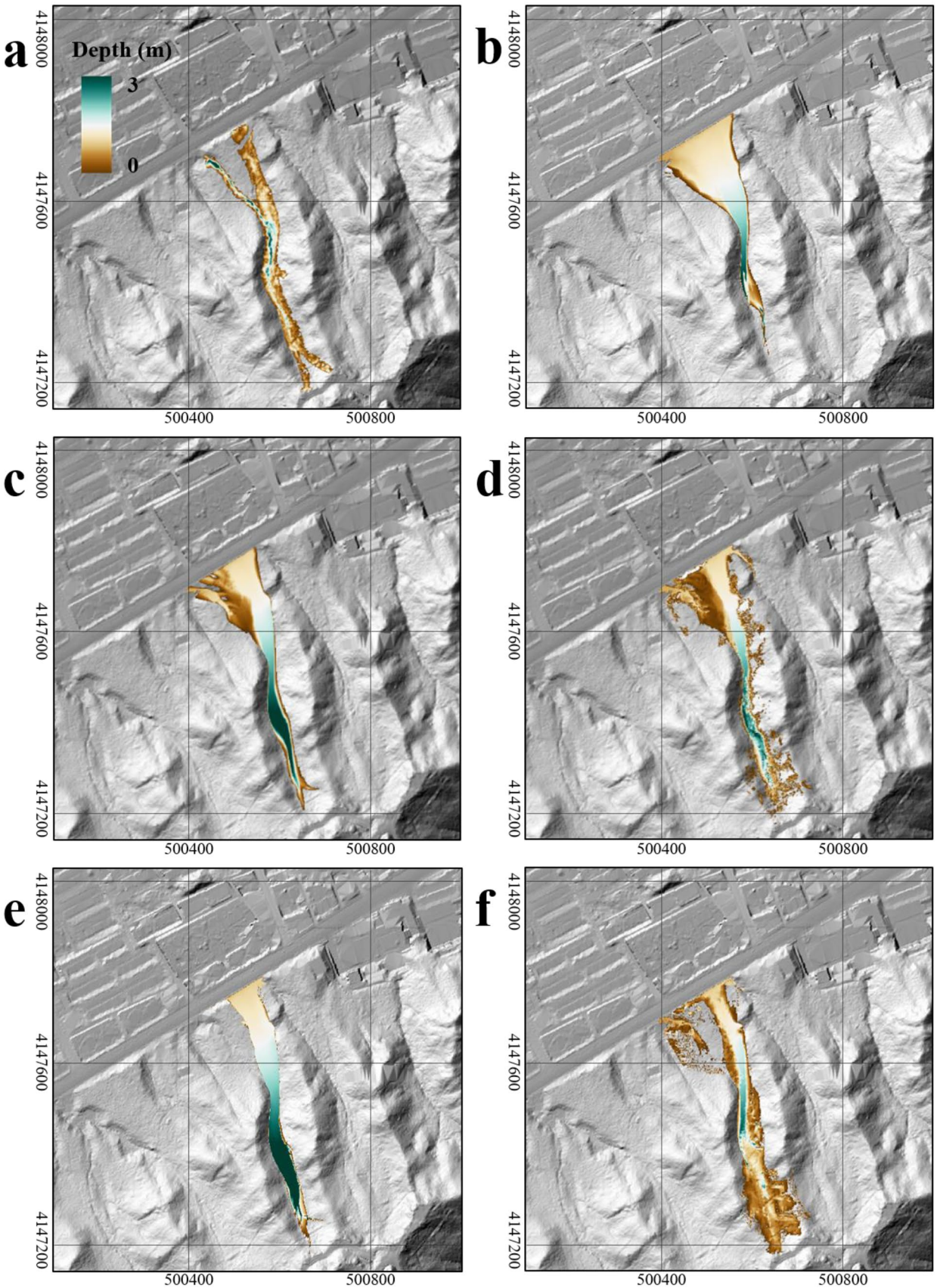

Fig. 4 Evaluation of modeled vs. observed erosion depth shape for the Raemian apartment basin based on the Voellmy rheological model. (**a**) Observation, (**b**) McDougall and Hungr (**c**) Sovilla, (**d**) Medina's static, (**e**) Medina's dynamic, and (**f**) Frank entrainment models

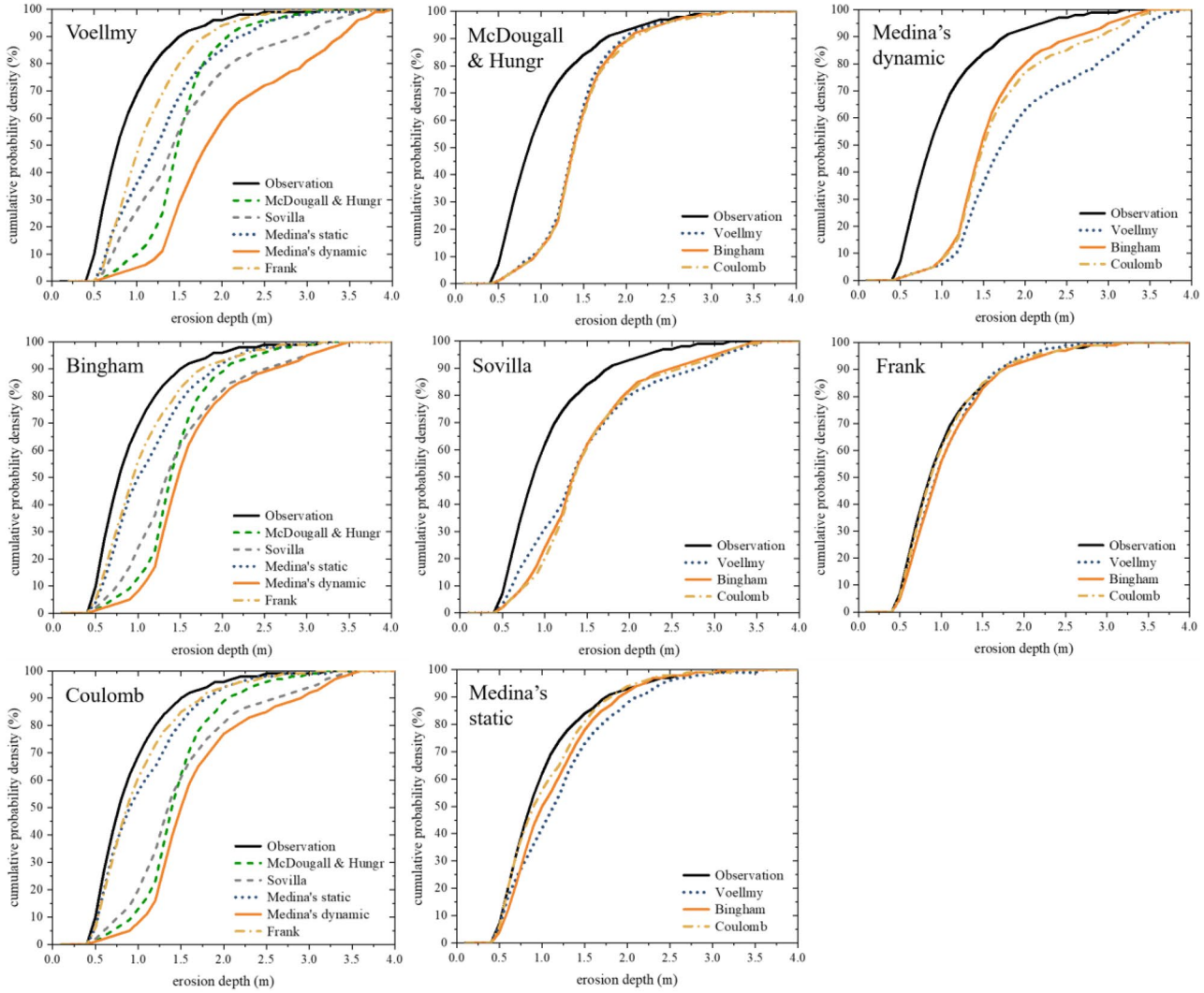

Fig. 5 Cumulative probability–density plot of modeled vs. observed erosion depths for the Raemian apartment basin based on a grid resolution of 1 m by 1 m (modified from Frank et al. 2015)

but it was analyzed that the erosion depth of 1 m or more is somewhat underestimated. The Voellmy and Frank combination result, which is the maximum debris-flow depths in the Sindonga basin, is shown in Fig. 9.

Discussion

The McDougall and Hungr entrainment model was designed to implement erosion–entrainment based on field data such as the initial volume, final volume, and length of the basin. And in the case of the Raemian and Sindonga apartment basins, all three parameters have been investigated through on-site surveys. However, it was difficult to simulate the debris-flow events, and it was necessary to calibrate the parameters. Finally, it appears that erosion–entrainment was more active in the study area than in McDougall and Hungr (2005). In the Sovilla model, the erosion–entrainment rates are governing factors. The larger the κ, the more active the erosion–entrainment, and the smaller the value, the less the erosion and entrainment action. In Medina's static model, parameter $dz/d\tau$ dominates the erosion and entrainment process. In the dynamic model, the flow velocity is in the denominator of the entrainment rate equation. This algorithm, Eq. (11), revealed an excessive erosion depth when the flow velocity was zero or close to zero. Therefore, to overcome this phenomenon, the study events were simulated by adopting the maximum entrainment rate. The Frank model demonstrated the best performance. In this algorithm, $dz/d\tau$ directly controlled the velocity of the erosion and entrainment process, and from the simulation results $dz/d\tau$ affected the erosion width, and τ_{fc} played a role similar to the critical point at which erosion–entrainment occurs.

Analyzing Figs. 5 and 8, it can be seen that selecting the rheological model was insignificant in implementing the erosion. In

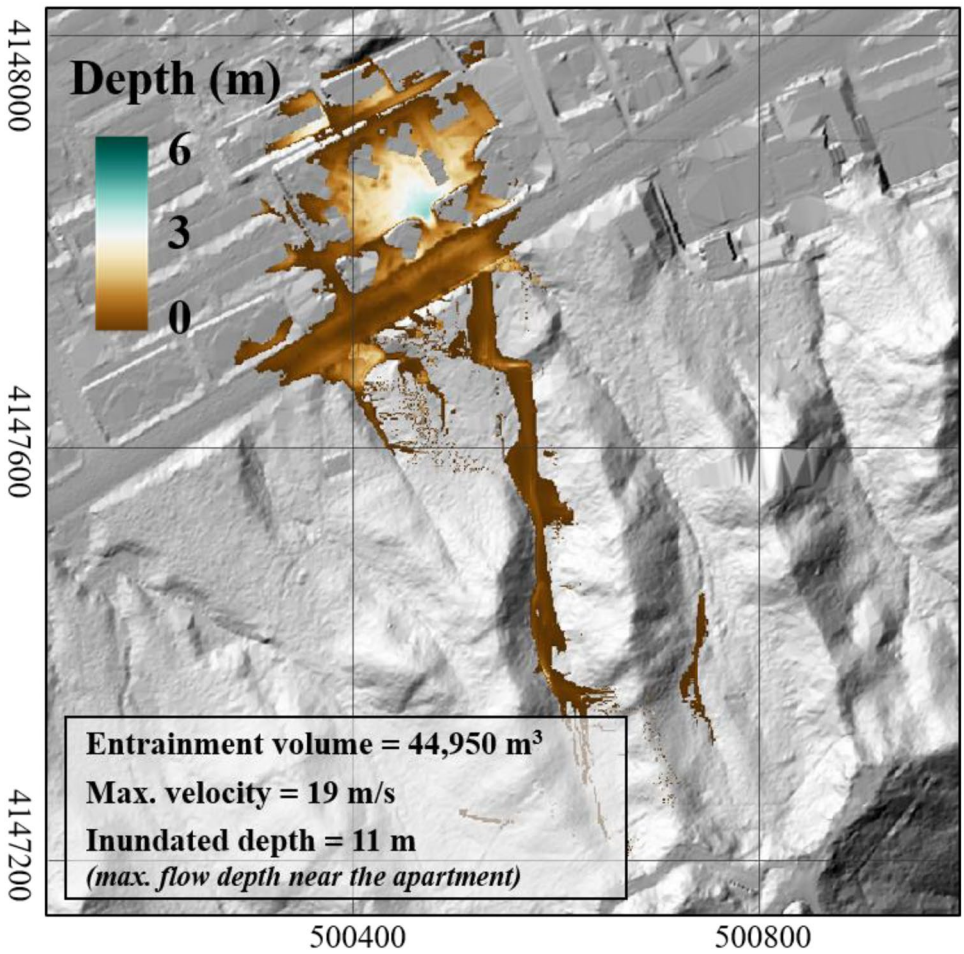

Fig. 6 The maximum flow depth at final in Raemian apartment basin analysis using Voellmy and Frank combination

contrast, the erosion–entrainment models dominated the erosion process regardless of rheological models. The algorithms of the erosion–entrainment model, analyzed in this study, can be divided into two types: 1) process-based entrainment rate approaches, such as McDougall and Hungr, Sovilla, and Medina's dynamic models, and 2) defined entrainment rate approaches as Medina's static and Frank models. In Figs. 4 and 7, the implemented erosion shape was divided into a smooth shape and an uneven shape. The erosion–entrainment algorithm exhibits flattened erosion patterns in Figs. 4b, c, 7b, and c, which included the flow velocity. Figures 4d, f, 7d, and f, which implemented erosion with a constant entrainment rate, show relatively irregular erosion patterns. In the case of Medina's dynamic model, unlike the McDougall and Sovilla models, the erosion aspect and depth were analogously implemented even though the flow velocity was located in the denominator, as shown in Eq. (11).

The A. E rate, summarized in Tables 1 and 2, is presented in Fig. 10. In Fig. 10a, the Coulomb-viscous rheological model most accurately simulated the experience of the Raemian and Sindonga apartment basins. The Voellmy model recorded the lowest A. E rate among the three rheological models; however, it exhibited a broad spectrum of A. E rate. Therefore, sufficient calibration was required when implementing debris flows using the Voellmy model. It is also unsuitable for simulating events with a rapid flow velocity (over 20 m/s).

In Fig. 10b, Medina's static and Frank erosion–entrainment model, designed with a constant entrainment rate (= erosion rate), simulated the event satisfactorily. In particular, the Frank model exhibited an exceedingly narrow spectrum and showed stable implementation results. Medina's dynamic model recorded the lowest A. E rate, but it was less stable than the Frank model. The Sovilla model with only one parameter showed the lowest accuracy, and the stability was also low, with a broad spectrum. Overall, McDougall and Hungr, Sovilla, and Medina's dynamic model, where the flow velocity was involved in the entrainment rate, exhibited a higher A. E rate than the models designed with a constant entrainment rate.

Limitation and further study

In this study, the erosion–entrainment algorithms are based on empirical or conceptual approaches and those models contain singularity because they are not derived in a physically and mathematically rigorous way. It should be noted that a mathematically consistent and mechanically correct erosion–entrainment model and modeling frame was recently proposed by Pudasaini and Fischer (2020) and Pudasaini and Krautblatter (2021). Their

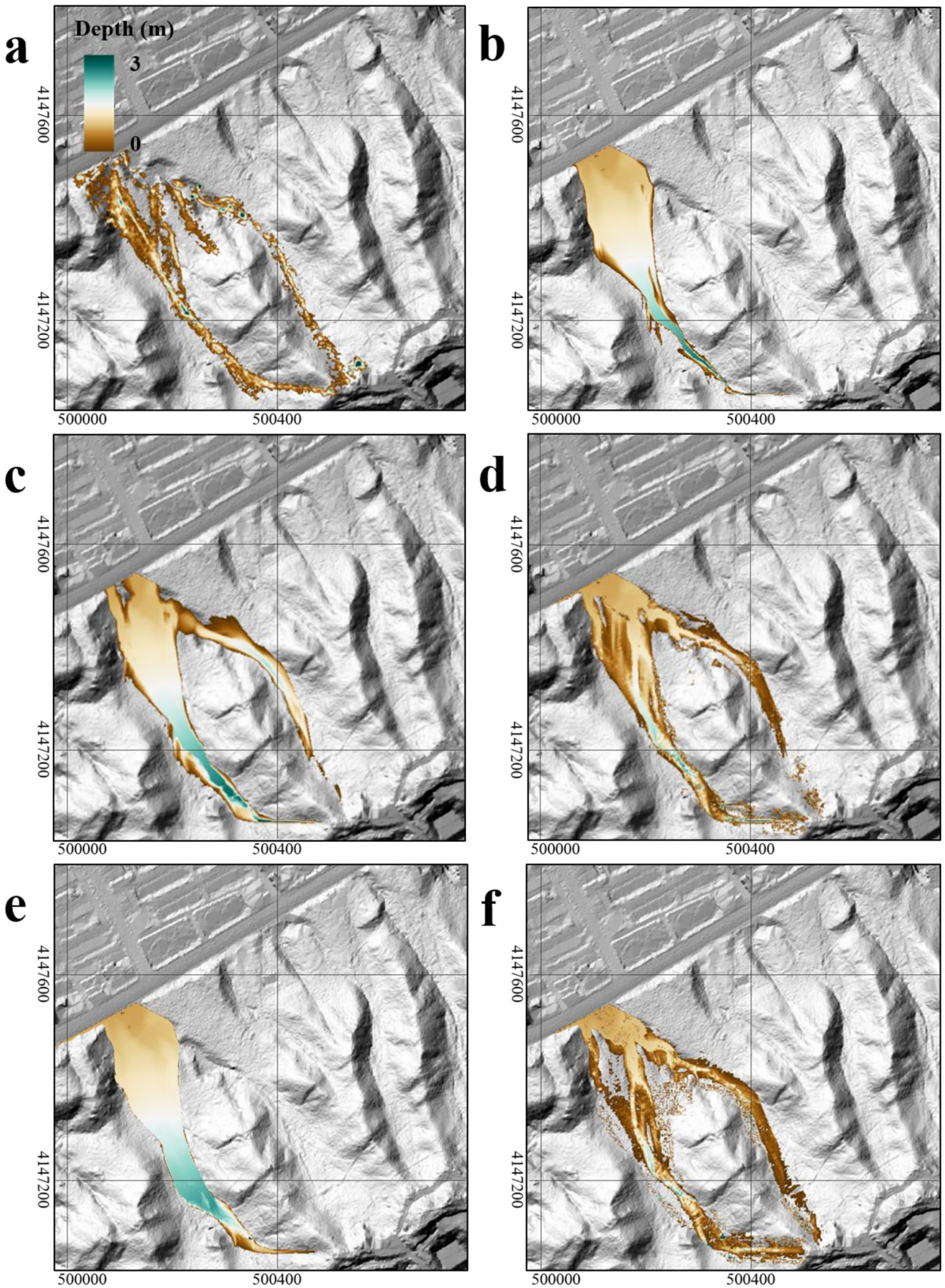

Fig. 7 Evaluation of modeled vs. observed erosion depth shape for the Sindonga apartment basin based on the Voellmy rheological model. (**a**) Observation, (**b**) McDougall and Hungr (**c**) Sovilla, (**d**) Medina's static, (**e**) Medina's dynamic, and (**f**) Frank entrainment models

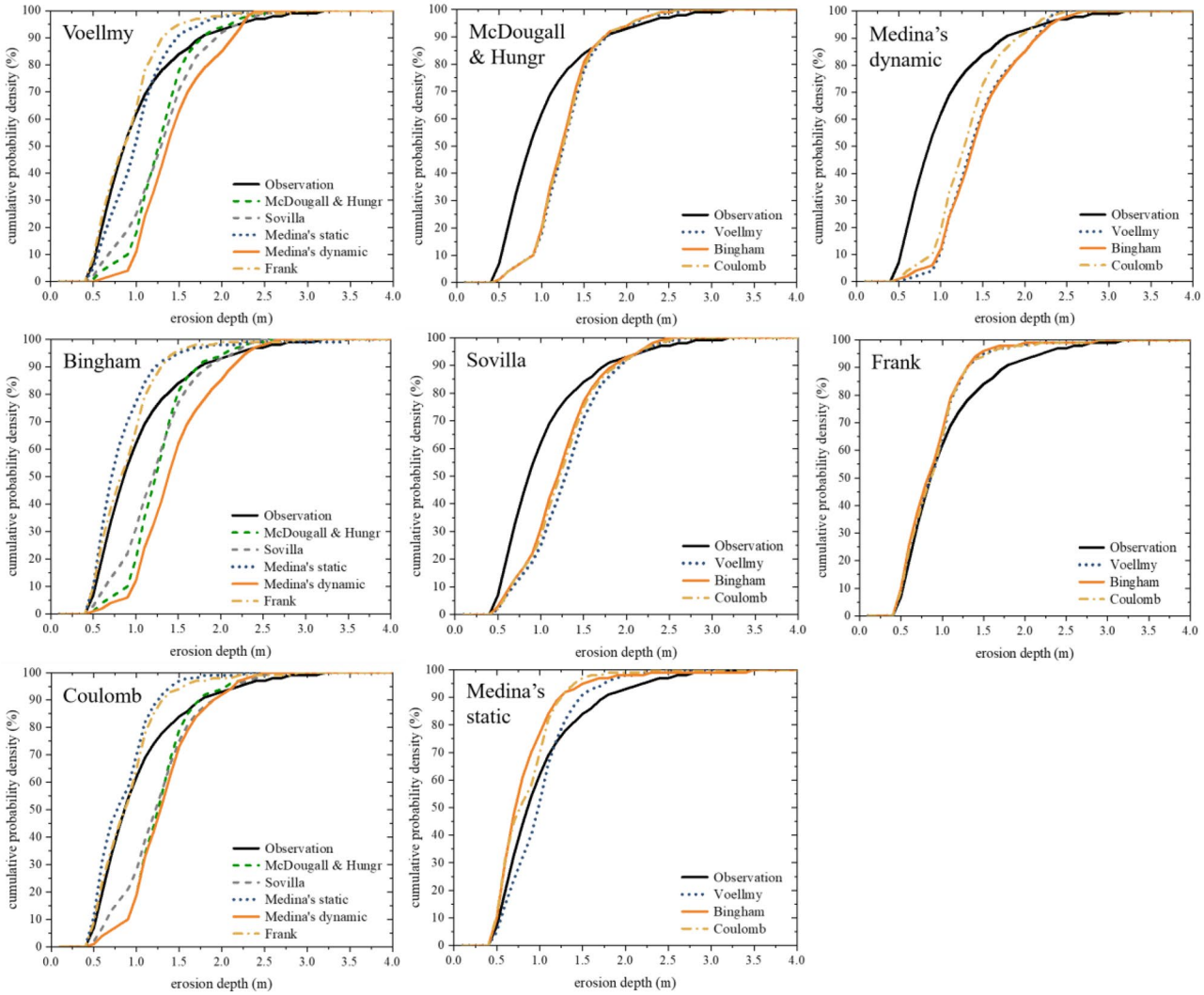

Fig. 8 Cumulative probability–density plot of modeled vs. observed erosion depths for the Sindonga apartment catchment based on a grid resolution of 1 m by 1 m (modified from Frank et al. 2015)

models enhance the momentum balance equations by including the erosion-induced inertia and the net momentum production and provide the first-ever mechanical condition for the mobility of erosive mass flows. Therefore, the next step required is to apply these physically and mathematically derived approaches because empirically based theories disregard the correct physical process (Pudasaini and Krautblatter 2021). In addition, the long-term analysis involving multiple debris-flow events needs to be investigated because it is proven that the erodible soil depth is highly affected by previous debris-flow events (Jakob et al. 2005). Thus, the erosion–entrainment algorithms based on empirical or conceptual approaches are often unable to explain the physical phenomenon of the erosion–entrainment process. Therefore, further research is required to identify other mechanisms of debris flows and sources of spatial variation in landslide susceptibility.

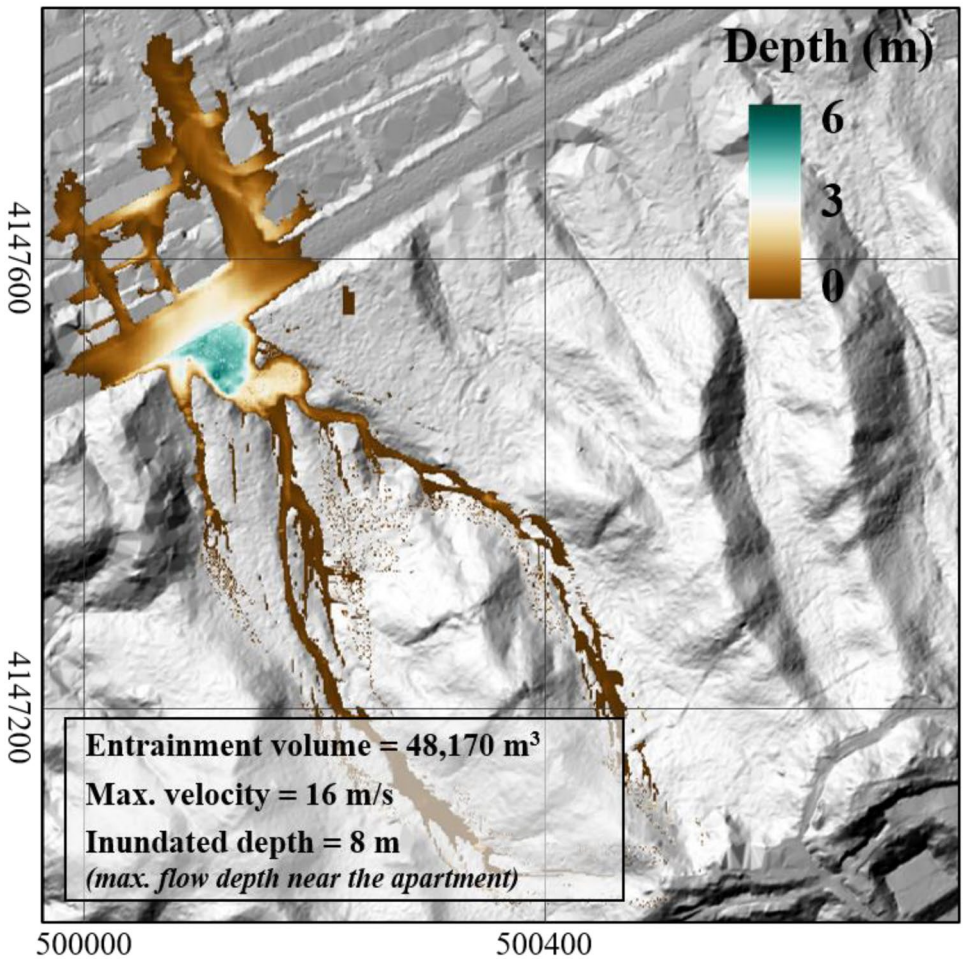

Fig. 9 The maximum flow depth at final in Sindonga apartment basin analysis using Voellmy and Frank combination

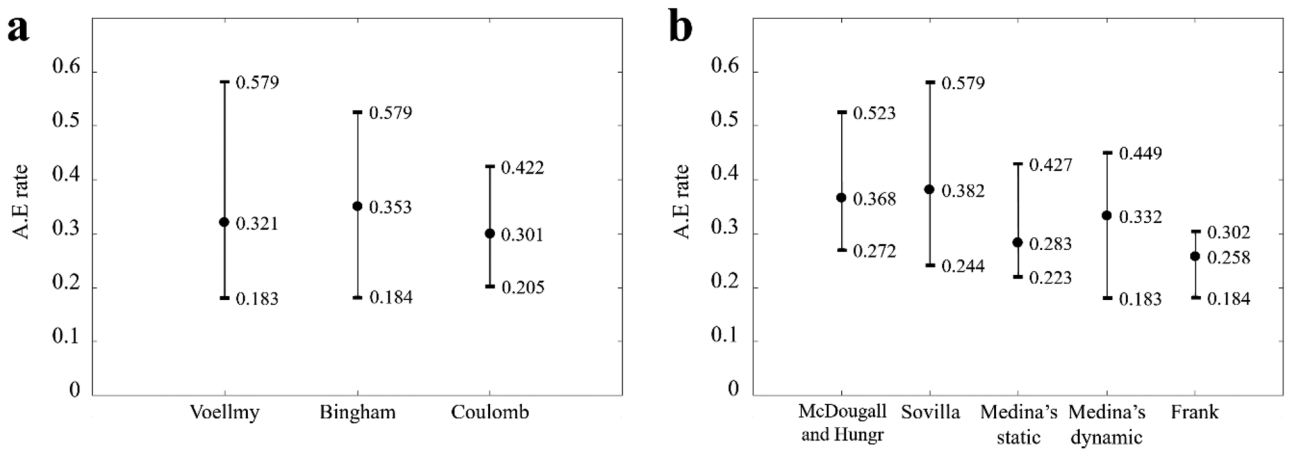

Fig. 10 Comprehensive A. E rate in the basin of Raemian and Sindonga apartments based on (**a**) rheological model and (**b**) erosion–entrainment model

Conclusions

The purpose of this study was to compare and analyze various erosion–entrainment models, McDougall and Hungr, Sovilla, Medina's static, Medina's dynamic, and Frank. Besides, the three rheological models (Voellmy, Bingham, and Coulomb-viscous) were used to analyze the difference according to the rheological model selection. The 2011 Mt. Umyeon landslides in the Republic of Korea were selected as the study event because it has considerable field survey data. The erosion–entrainment models had a dominant effect on the implementation of the erosion shape, while the choice of the rheological model was insignificant. The simulation results of the erosion–entrainment model, designed with a constant entrainment rate, exhibited higher accuracy. Particularly, the implementation results of the Frank erosion–entrainment model showed stable and superior accuracy compared to other models. The result of this study can be useful for the selection of the erosion model in debris-flow prediction or scenario-based simulation.

Acknowledgments

This work was supported by Korea Hydro and Nuclear Power Co., Ltd. (No. 2018-Tech-19) and the Basic Research Project of the Korea Institute of Geoscience and Mineral Resources (Project code: 22-3412-1).

Declarations

Competing interests The authors declare no known competing financial interests or personal relationships that could have appeared to influence the work reported in this research.

References

Abraham MT, Satyam N, Reddy SKP, Pradhan B (2021) Runout modeling and calibration of friction parameters of Kurichermala debris flow, India. Landslides 18:737–754. https://doi.org/10.1007/s10346-020-01540-1

An H, Ichikawa Y, Tachikawa Y, Shiiba M (2012) Comparison between iteration schemes for three-dimensional coordinate-transformed saturated–unsaturated flow model. J Hydrol 470:212–226. https://doi.org/10.1016/j.jhydrol.2012.08.056

An H, Kim M, Lee G, Kim Y, Lim H (2019) Estimation of the area of sediment deposition by debris flow using a physical-based modeling approach. Quat Int 503:59–69. https://doi.org/10.1016/j.quaint.2018.09.049

Audusse E, Bouchut F, Bristeau M-O, Klein R, Perthame BT (2004) A Fast and Stable Well-Balanced Scheme with Hydrostatic Reconstruction for Shallow Water Flows. SIAM J Sci Comput 25:2050–2065. https://doi.org/10.1137/s1064827503431090

Bartelt P, Buehler Y, Christen M, Deubelbeiss Y, Graf C, McArdell B (2013) RAMMS–rapid mass movement simulation, A modeling system for debris flows in research and practice, user manual v1. 5, debris flow, manuscript update: 31 January 2013. WSL Institute for Snow and Avalanche Research SLF, available at: http://ramms.slf.ch/ramms/downloads/RAMMS_DBF_Manual.pdf. Accessed 27 Feb 2015

Bertolo P, Bottino G (2008) Debris-flow event in the Frangerello Stream-Susa Valley (Italy)—calibration of numerical models for the back analysis of the 16 October, 2000 rainstorm. Landslides 5:19–30. https://doi.org/10.1007/s10346-007-0099-7

Bingham EC (1922) Fluidity and plasticity. McGraw Hill, New York, p 440

Cepeda J, Chávez JA, Martínez CC (2010) Procedure for the selection of runout model parameters from landslide back-analyses: application to the Metropolitan Area of San Salvador, El Salvador. Landslides 7:105–116. https://doi.org/10.1007/s10346-010-0197-9

Cesca M, D'Agostino V (2008) Comparison between FLO-2D and RAMMS in debris-flow modelling: a case study in the Dolomites. WIT Trans Eng Sci 60:197–206. https://doi.org/10.2495/deb080201

Christen M, Kowalski J, Bartelt P (2010) RAMMS: Numerical simulation of dense snow avalanches in three-dimensional terrain. Cold Reg Sci Technol 63:1–14. https://doi.org/10.1016/j.coldregions.2010.04.005

Coe JA, Kean JW, Godt JW, Baum RL, Jones ES, Gochis DJ, Anderson GS (2014) New insights into debris-flow hazards from an extraordinary event in the Colorado Front Range. GSA Today 24:4–10. https://doi.org/10.1130/GSATG214A.1

Dahl M-PJ, Gauer P, Kalsnes BG, Mortensen LE, Jensen NH, Veihe A (2013) Numerical runout simulation of debris avalanches in the Faroe Islands, North Atlantic Ocean. Landslides 10:623–631. https://doi.org/10.1007/s10346-012-0355-3

Denlinger RP, Iverson RM (2001) Flow of variably fluidized granular masses across three-dimensional terrain: 2. Numerical predictions and experimental tests. J Geophys Res 106:553–566. https://doi.org/10.1029/2000JB900330

Fawcett T (2006) An introduction to ROC analysis. Pattern Recognit Let 27:861–874. https://doi.org/10.1016/j.patrec.2005.10.010

Frank F, McArdell BW, Huggel C, Vieli A (2015) The importance of entrainment and bulking on debris flow runout modeling: examples from the Swiss Alps. Nat Hazards Earth Syst Sci 15:2569–2583. https://doi.org/10.5194/nhess-15-2569-2015

Godt JW, Baum RL, Savage WZ, Salciarini D, Schulz WH, Harp EL (2008) Transient deterministic shallow landslide modeling: Requirements for susceptibility and hazard assessments in a GIS framework. Eng Geol 102:214–226. https://doi.org/10.1016/j.enggeo.2008.03.019

Hong M, Jeong S, Kim J (2020) A combined method for modeling the triggering and propagation of debris flows. Landslides 17:805–824. https://doi.org/10.1007/s10346-019-01294-5

Hussin HY, Quan Luna B, Van Westen CJ, Christen M, Malet J-P, Van Asch TWJ (2012) Parameterization of a numerical 2-D debris flow model with entrainment: a case study of the Faucon catchment, Southern French Alps. Nat Hazards Earth Syst Sci 12:3075–3090. https://doi.org/10.5194/nhess-12-3075-2012

Iverson RM (1997) The physics of debris flows. Rev Geophys 35:245–296. https://doi.org/10.1029/97rg00426

Iverson RM, Denlinger RP (2001) Flow of variably fluidized granular masses across three-dimensional terrain: 1. Coulomb Mixture Theory J Geophys Res 106:537–552. https://doi.org/10.1029/2000JB900329

Jakob M, Bovis M, Oden M (2005) The significance of channel recharge rates for estimating debris-flow magnitude and frequency. Earth Surf Process Landf 30:755–766. https://doi.org/10.1002/esp.1188

Johnson AM, Rodine JR (1984) Debris flow: slope instability, edited by Brunsden D and Prior DB. Wiley 257–361

Kean JW, Staley DM, Cannon SH (2011) In situ measurements of post-fire debris flows in southern California: Comparisons of the timing and magnitude of 24 debris-flow events with rainfall and soil moisture conditions. J Geophys Res 116:F04019. https://doi.org/10.1029/2011jf002005

Lai J, Wang G, Wang Z, Chen J, Pang X, Wang S, Zhou Z, He Z, Qin Z, Fan X (2018) A review on pore structure characterization in tight sandstones. Earth Sci Rev 177:436–457. https://doi.org/10.1016/j.earscirev.2017.12.003

Lee S, An H, Kim M, Lim H (2020) Analysis of debris flow simulation parameters with entrainment effect: a case study in the Mt. Umyeon J Korea Water Resour Assoc 53:637–646. https://doi.org/10.3741/JKWRA.2020.53.9.637

Liu W, He S (2020) Comprehensive modelling of runoff-generated debris flow from formation to propagation in a catchment. Landslides 17:1529–1544. https://doi.org/10.1007/s10346-020-01383-w

McDougall S, Hungr O (2005) Dynamic modelling of entrainment in rapid landslides. Can Geotech J 42:1437–1448. https://doi.org/10.1139/t05-064
Medina V, Hürlimann M, Bateman A (2008) Application of FLATModel, a 2D finite volume code, to debris flows in the northeastern part of the Iberian Peninsula. Landslides 5:127–142. https://doi.org/10.1007/s10346-007-0102-3
Mergili M, Jaboyedoff M, Pullarello J, Pudasaini SP (2020a) Back calculation of the 2017 Piz Cengalo-Bondo landslide cascade with r.avaflow: what we can do and what we can learn. Nat Hazards Earth Syst Sci 20:505–520. https://doi.org/10.5194/nhess-20-505-2020
Mergili M, Pudasaini SP, Emmer A, Fischer JT, Cochachin A, Frey H (2020b) Reconstruction of the 1941 GLOF process chain at Lake Palcacocha (Cordillera Blanca, Peru). Hydrol Earth Syst Sci 24:93–114. https://doi.org/10.5194/hess-24-93-2020
Morgenstern NR (1978) Mobile soil and rock flows. Lecture given at the fifth Southeast Asian Conference on soil engineering, Bangkok, July 1977. Geotech Eng 9(2):123–141
Naef D, Rickenmann D, Rutschmann P, McArdell BW (2006) Comparison of flow resistance relations for debris flows using a one-dimensional finite element simulation model. Nat Hazards Earth Syst Sci 6:155–165. https://doi.org/10.5194/nhess-6-155-2006
Pirulli M (2010) On the use of the calibration-based approach for debris-flow forward-analyses. Nat Hazards Earth Syst Sci 10:1009–1019. https://doi.org/10.5194/nhess-10-1009-2010
Pirulli M, Sorbino G (2008) Assessing potential debris flow runout: a comparison of two simulation models. Nat Hazards Earth Syst Sci 8:961–971. https://doi.org/10.5194/nhess-8-961-2008
Pitman EB, Patra A, Bauer A, Sheridan M, Bursik M (2003) Computing debris flows and landslides. Phys Fluids 15:3638–3646
Pudasaini SP (2012) A general two-phase debris flow model. J Geophys Res Earth Surf 117:F03010. https://doi.org/10.1029/2011JF002186
Pudasaini SP, Mergili M (2019) A multi-phase mass flow model. J Geophys Res 124:2920–2942. https://doi.org/10.1029/2019JF005204
Pudasaini SP, Fischer JT (2020) A mechanical erosion model for two-phase mass flows. Int J Multiph Flows 132:103416. https://doi.org/10.1016/j.ijmultiphaseflow.2020.103416
Pudasaini SP, Krautblatter M (2021) The mechanics of landslide mobility with erosion. Nat Commun 12:6793. https://doi.org/10.1038/s41467-021-26959-5
Pudasaini SP, Wang Y, Hutter K (2005) Modelling debris flows down general channels. Nat Hazards Earth Syst Sci 5:799–819. https://doi.org/10.5194/nhess-5-799-2005
Remaître A, Malet J-P, Maquaire O (2005) Morphology and sedimentology of a complex debris flow in a clay-shale basin. Earth Surf Process Landf 30:339–348. https://doi.org/10.1002/esp.1161
Rickenmann D, Laigle D, McArdell BW, Hübl J (2006) Comparison of 2D debris-flow simulation models with field events. Comput Geosci 10:241–264. https://doi.org/10.1007/s10596-005-9021-3
Scaringi G, Fan X, Xu Q, Liu C, Ouyang C, Domènech G, Yang F, Dai L (2018) Some considerations on the use of numerical methods to simulate past landslides and possible new failures: the case of the recent Xinmo landslide (Sichuan, China). Landslides 15:1359–1375. https://doi.org/10.1007/s10346-018-0953-9
Seoul City (2014) Research contract report: Addition and Complement causes survey of Mt, vol. 2011 Woomyeon landslide (In Korean)
Shugar DH, Jacquemart M, Shean D et al (2021) A massive rock and ice avalanche caused the 2021 disaster at Chamoli. Indian Himalaya Sci 373(6552):300–306. https://doi.org/10.1126/science.abh4455
Sovilla B, Burlando P, Bartelt P (2006) Field experiments and numerical modeling of mass entrainment in snow avalanches. J Geophys Res 111:F03007. https://doi.org/10.1029/2005JF000391
Stock J, Dietrich WE (2003) Valley incision by debris flows: Evidence of a topographic signature. Water Resour Res 39:1089. https://doi.org/10.1029/2001wr001057
Takahashi T (2007) Debris flow: mechanics, prediction and countermeasures. Taylor and Francis, New York
Takahashi T, Nakagawa H (1991) Prediction of stony debris flow induced by severe rainfall. J Jpn Soc Eros Control Eng 44:12–19. https://doi.org/10.11475/sabo1973.44.3_12
Voellmy A (1955) Über die Zerstörungskraft von Lawinen. Schweiz Bauztg 73:212–285

Seungjun Lee · Hyunuk An (✉)
Department of Agricultural and Rural Engineering, Chungnam National University, Daejeon, Republic of Korea
Email: hyunuk@cnu.ac.kr

Minseok Kim (✉)
Geologic Hazards Division, Korea Institute of Geoscience and Mineral Resources, Daejeon, Republic of Korea
Email: minseok_kim@kigam.re.kr

Giha Lee
Department of Advanced Science and Technology Convergence, Kyungpook National University, Sangju, Republic of Korea

Hongjoon Shin
Hydro-Power Research and Training Center, Korea Hydro and Nuclear Power Co., LTD, Gyeonggi-do, Republic of Korea